Supplementary Information

Fe Containing Templates Derived Atomic Fe-N-C to Boost Fenton-Like Reaction and the Charge Migration Analysis on Highly Active Fe-N_4 Sites

Yuan Gao,[a] Xiaoguang Duan,[b] Bin Li,[a] Qianqian Jia,[a] Yang Li,[a] Xiaobin Fan,[a] Fengbao Zhang,[a] Guoliang Zhang,[a] Shaobin Wang [b] and Wenchao Peng *[a]

[a] School of Chemical Engineering and Technology, Tianjin University, Tianjin 300350, China.
[b] School of Chemical Engineering and Advanced Materials, The University of Adelaide, Adelaide SA 5005, Australia

*Corresponding author: Wenchao Peng. E-mail: wenchao.peng@tju.edu.cn

Text S1. Density functional theory calculations

The models were computed with density functional theory (DFT) using projected augment wave method as implemented in the Vienna ab initio Simulation Package (VASP) code.[1,2] The generalized gradient approximation (GGA) of Perdew-Burke-Ernzerhof (PBE) is used for the exchange-correlation potential.[3] Plane-wave basis set was used with an energy cutoff of 450 eV. The convergence criterion for electronic structure iteration was set to be 1×10^{-4} eV, and structural optimization would be terminated until all the forces were smaller than 0.05eV/Å. Polarization effect was considered. The charge transfer was analyzed by calculating the charge density using the Bader charge analysis method.[4] Vacuum slab was set to be 17 Å to avoid interactions between adjacent layers, k-mesh was set as 2×2×1 in this work. The adsorption energy was defined as:

$E_{ads} = E_{slab+PMS} - E_{slab} - E_{PMS}$

where $E_{slab+PMS}$ was the total energy of the model; E_{slab} was the energy of the surface of catalyst; E_{PMS} was the energy of free PMS.[5,6]

During the DFT calculations, several different adsorption configurations of PMS molecule on Fe-N_4 active sites have been established. The detailed explanations of each adsorption model are described as follows:

Firstly, the model of PMS molecule with labeled O atoms is shown in Fig. S23. Type 1 is the fully relaxed adsorption configuration of PMS on Fe-N_4 sites (Fig. 9a), the initial position of PMS molecules is above Fe atom and the O^1 atom is adsorbed on Fe atom. Type 2, 3 are adsorption configuration with the initial positions of PMS molecules above N, C atom in Fe-N_4-C_x structure (Fig. 9a-c). Type 4 is same as Type 1 except that the O-O bond of PMS molecules is parallel to the plane of carbon skeleton (Fig. 9d). Type 5, 6, 7 are adsorption configurations with adsorption of O^2, O^3, O^4 atoms on Fe atom respectively (Fig. 9e-g). In addition, the initial positions of PMS molecule in Type 4-7 are all above Fe atom.

Text S2

Generally, the deactivation of metal/carbon materials is mainly attributed to the leaching of metal, the electronic state changes leaded by oxidation of non-metal active sites, and the blocking of surface active sites caused by adsorption of organic pollutants and their intermediates. In this work, it is interesting that the weight of the activator has been significantly increased after each reuse (Table S6). Considering the adsorbed intermediates could be removed during the washing, the weight increasing should be due to the oxidation of the materials and many oxygen-containing functional groups are bonded to the carbon atoms on the surface. As shown in Fig. S19a, the diffraction peak at 22° becomes broader, indicating the decreasing of crystallinity. Raman spectroscopy shows that the I_D/I_G gradually decreases from 1.05 (fresh activator) to 0.68 (after 5th run) (Fig. S19b), suggesting that the degradation process reduces the defect level of the activator. According to the FT-IR spectroscopy (Fig. S19c), after 5 recycles, the characteristic peaks of C=O and C-O is significantly increased compared with fresh activator, indicating the oxidation of carbon structure. As shown in XPS spectra (Fig. S20a), O content increases from 4.52 at% to 19.64 at%, N content decreases from 8.87 at% to 2.35 at% and Fe content decreases from 0.16 at% to 0.08 at% (Table S7). The high-resolution spectrums of C 1s and O 1s show the content change of different oxygen-containing functional groups (Fig. S20b-c). These results could prove that material is oxidized and many oxygen-containing groups are bonded to carbon skeleton during the degradation process. In addition, the ratios of pyridinic N and graphitic N decrease to 15.6% and 18.3% respectively (Fig. S20d), indicating the reduction of effective N active sites. Therefore, the material deactivation could be mainly attributed to: (1) The oxidation of the carbon atoms breaks the sp^2 carbon framework, which could decrease the conductivity and inhibit the electron transfer. (2) The loss of graphitic and pyridinic N reduce the active sites for PMS activation. (3) The leaching of Fe species on the surface or the cover by surface oxygen groups and reaction intermediates.

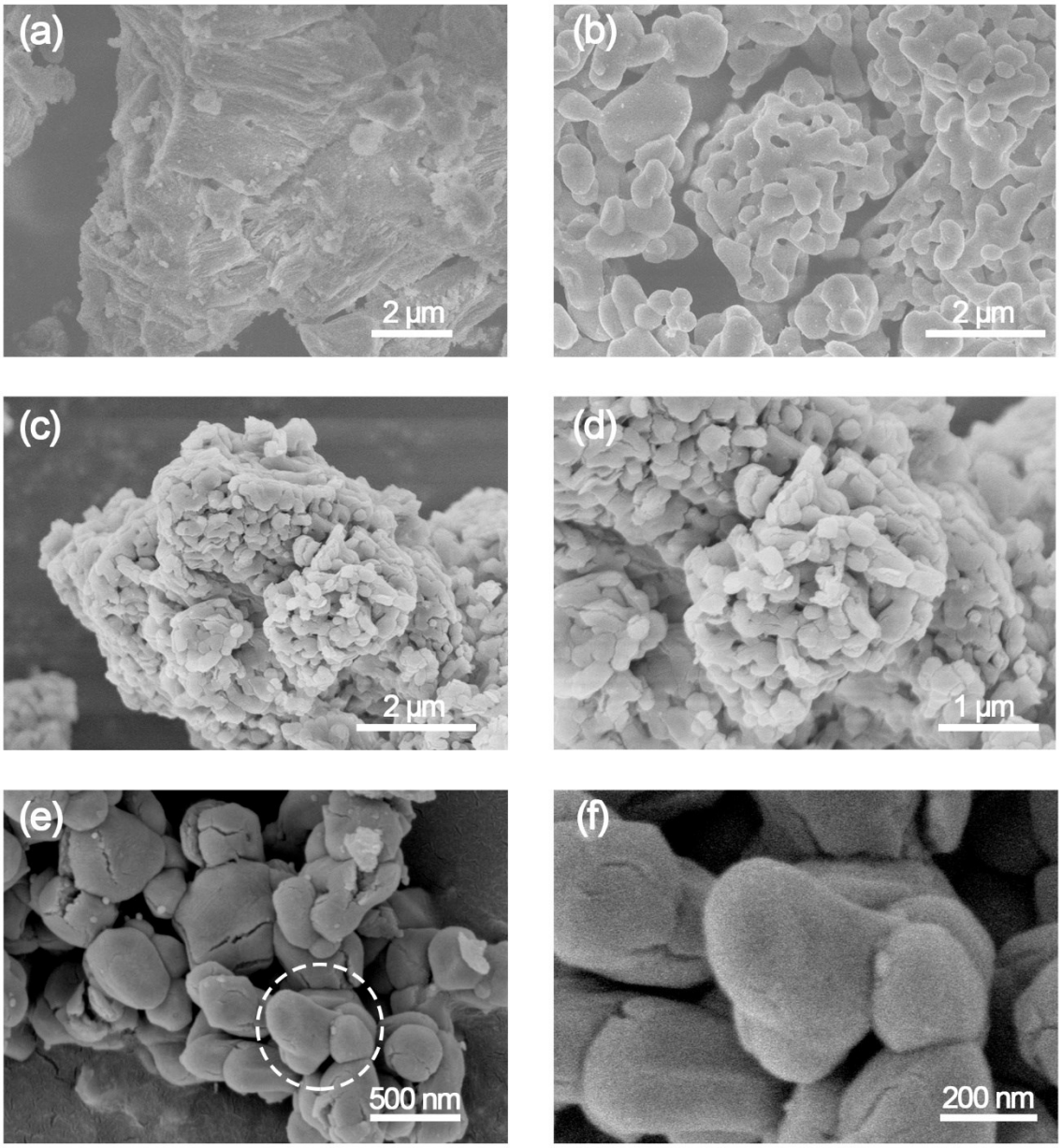

Fig. S1 SEM images of (a) commercial $Ca(OH)_2$, (b) calcined CaO and (c-f) Fe@CaO-30.

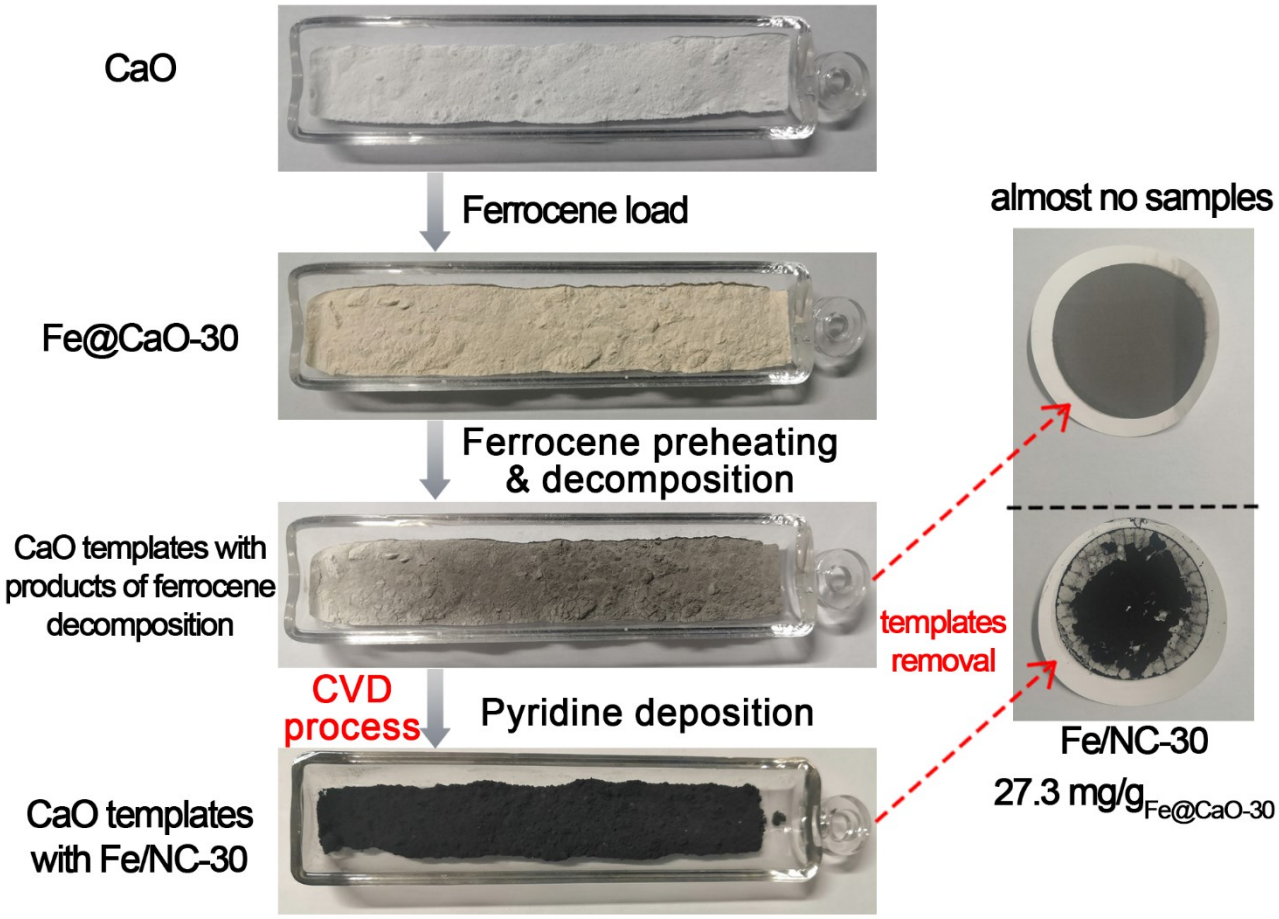

Fig. S2 The images of samples obtained after each step in the materials synthesis processes.

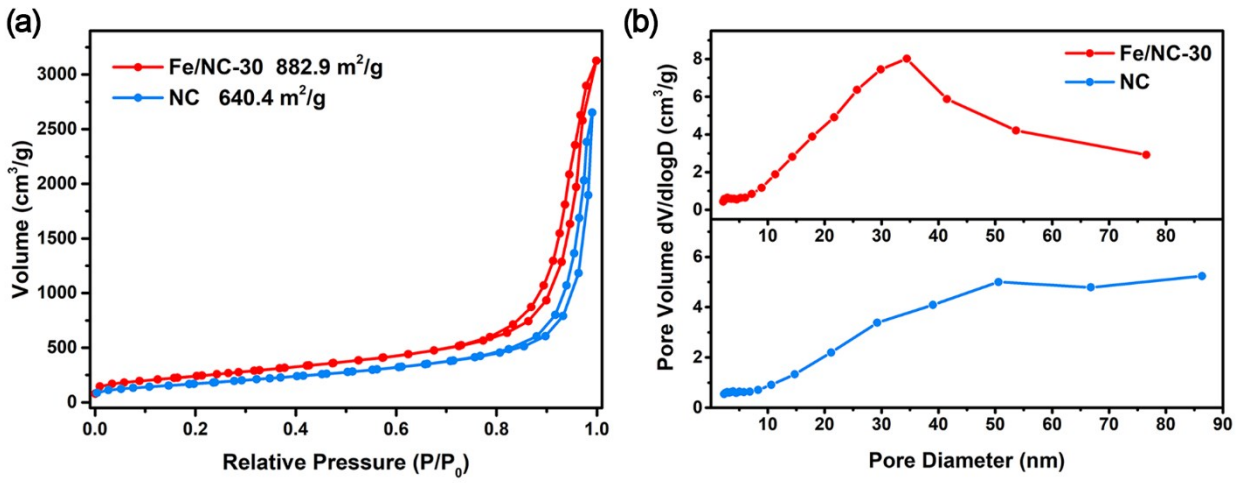

Fig. S3 (a) Nitrogen adsorption-desorption isotherms and (b) corresponding pore size distributions of Fe/NC-30 and NC in the other batch.

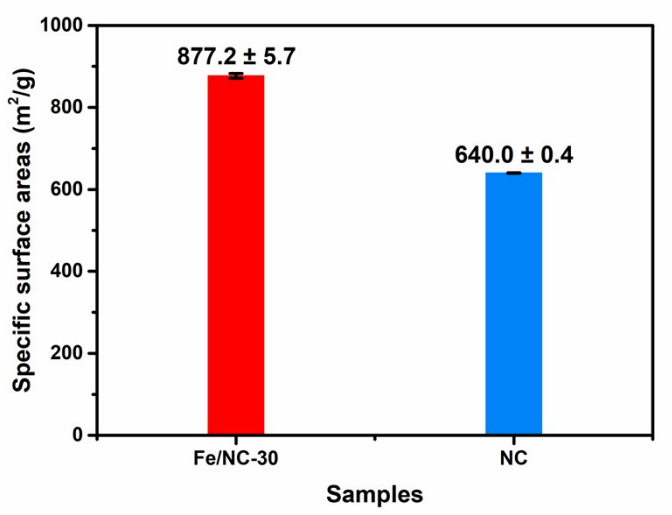

Fig. S4 The specific surface areas (SSAs) with error bar of Fe/NC-30 and NC samples.

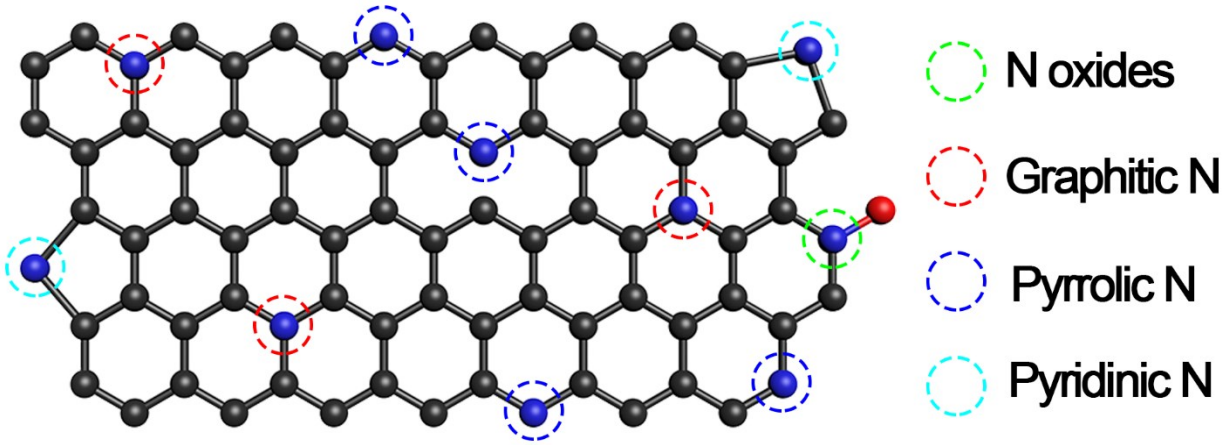

Fig. S5 The bonding schematic diagram of NC sample.

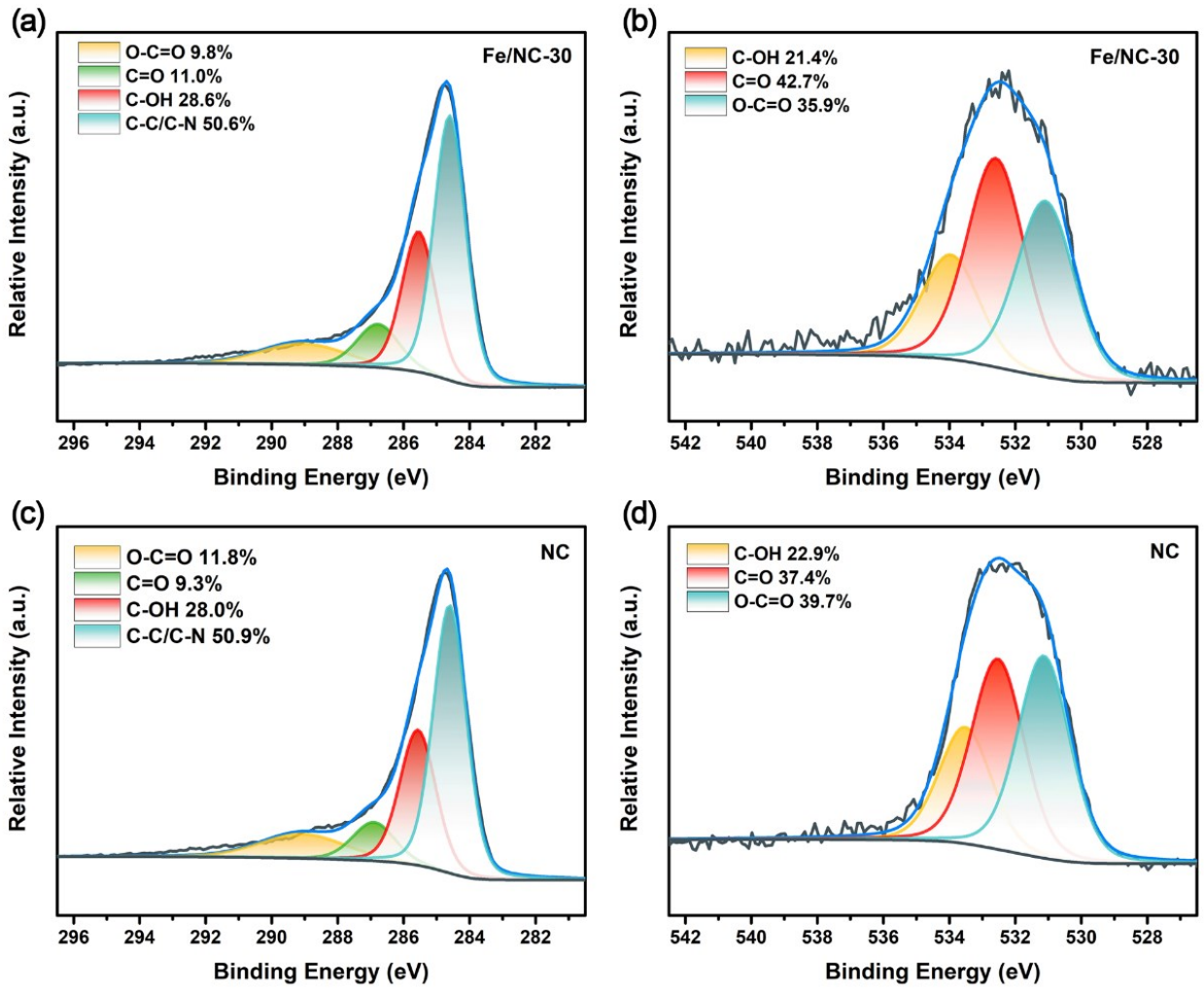

Fig. S6 (a) C 1s spectra and (b) O 1s spectra of Fe/NC-30. (c) C 1s spectra and (d) O 1s spectra of NC.

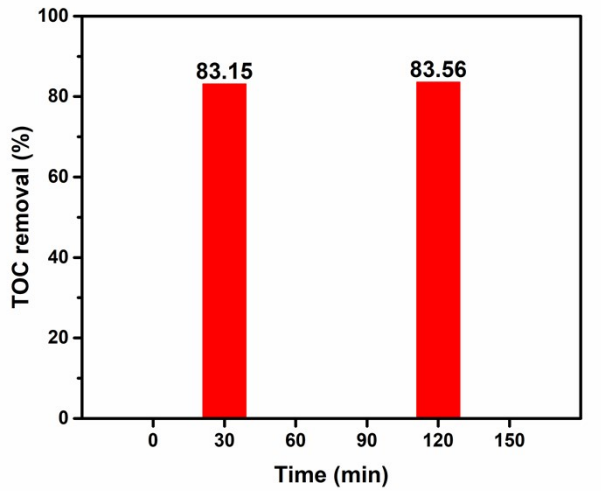

Fig. S7 TOC removal with Fe/NC-30 as activator in 30 and 120 min. (The reaction conditions: [phenol] = 50 ppm, [activator] = 25 mg/L, [PMS] = 1.0 g/L, T = 25 ºC.)

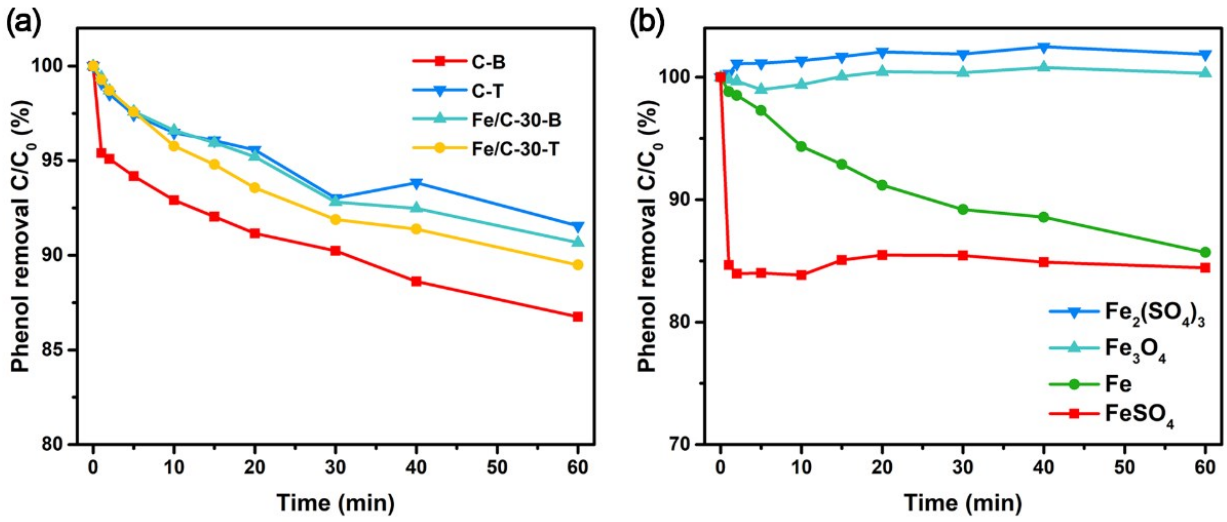

Fig. S8 Phenol removal on (a) different nitrogen-free activators and (b) Fe elements and different compounds. ([activator] = [other Fe species] = 25 mg/L.)

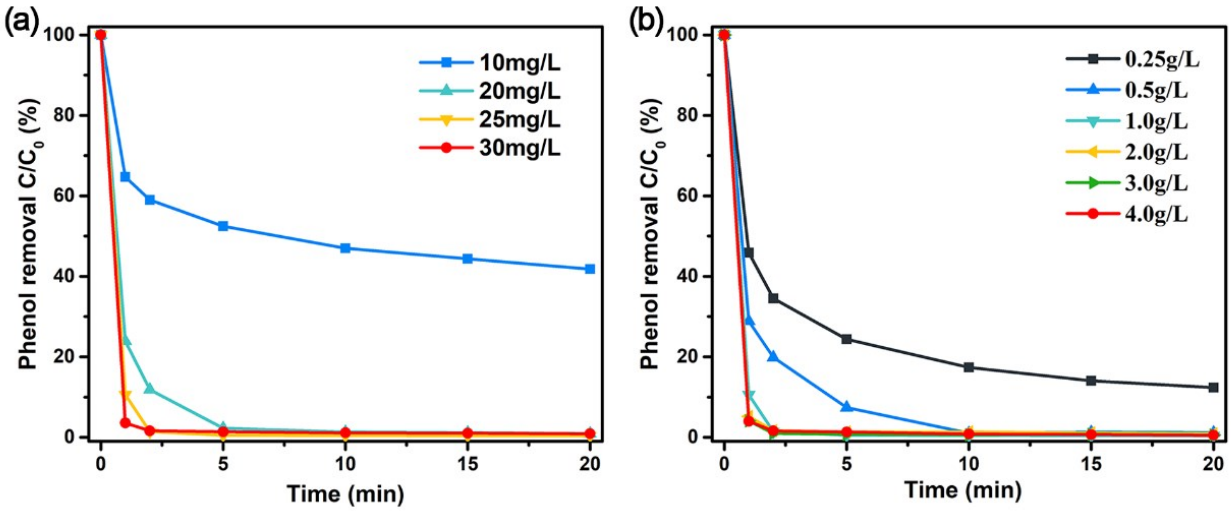

Fig. S9 The effects of (a) activator concentration and (b) PMS dosage on phenol degradation with Fe/NC-30 as activator. (The reaction conditions: [phenol] = 50 ppm, [activator] = 25 mg/L, [PMS] = 1.0 g/L, T = 25 ºC. All other conditions remain unchanged except for the variables to be studied.)

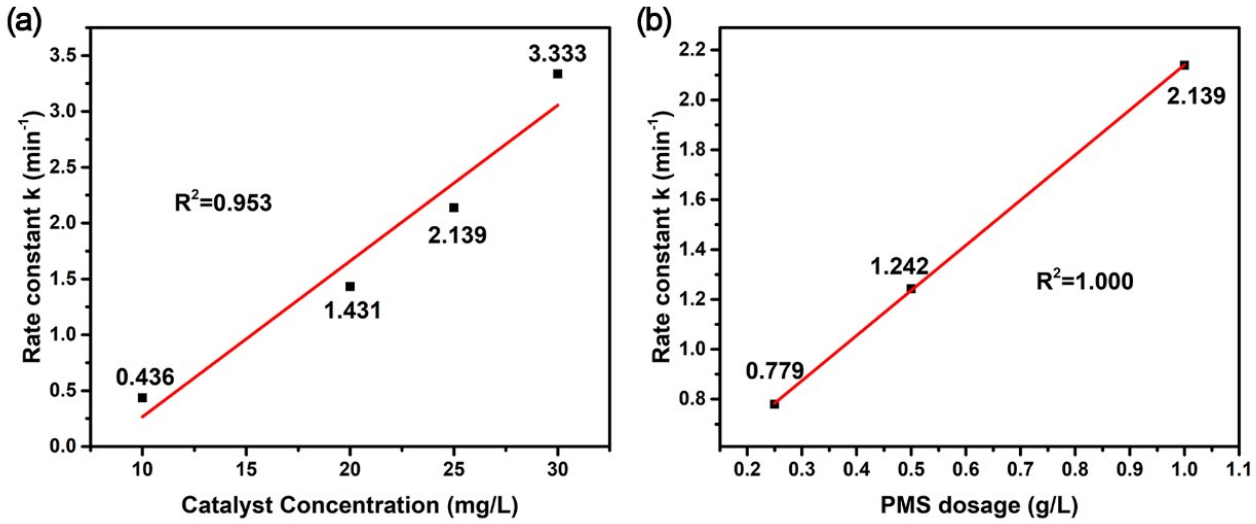

Fig. S10 Linear fit of reaction rate constants to (a) activator concentration and (b) PMS dosage of Fe/NC-30.

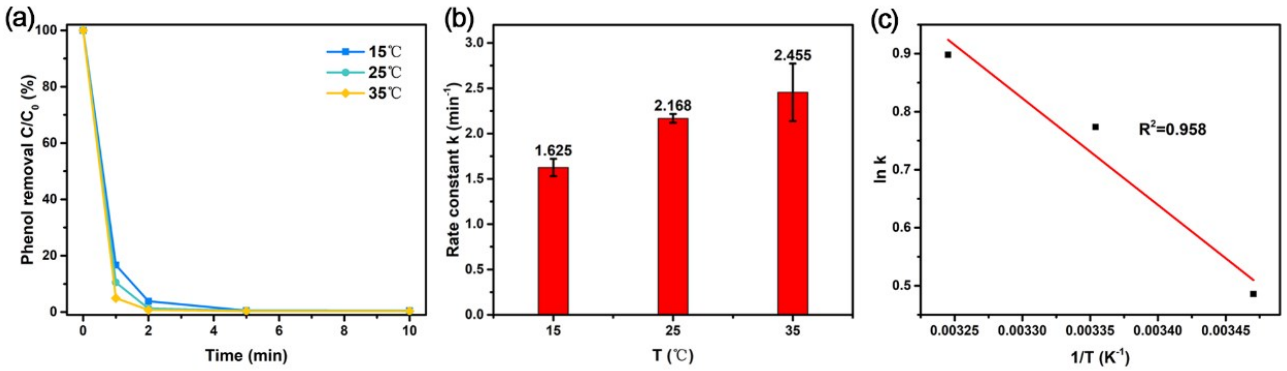

Fig. S11 (a) The effects of reaction temperature on phenol degradation with Fe/NC-30 as activator. (b) Corresponding reaction rate constants at different temperature. (c) Linear fit of activation energy of Fe/NC-30. (The reaction conditions: [phenol] = 50 ppm, [activator] = 25 mg/L, [PMS] = 1.0 g/L.)

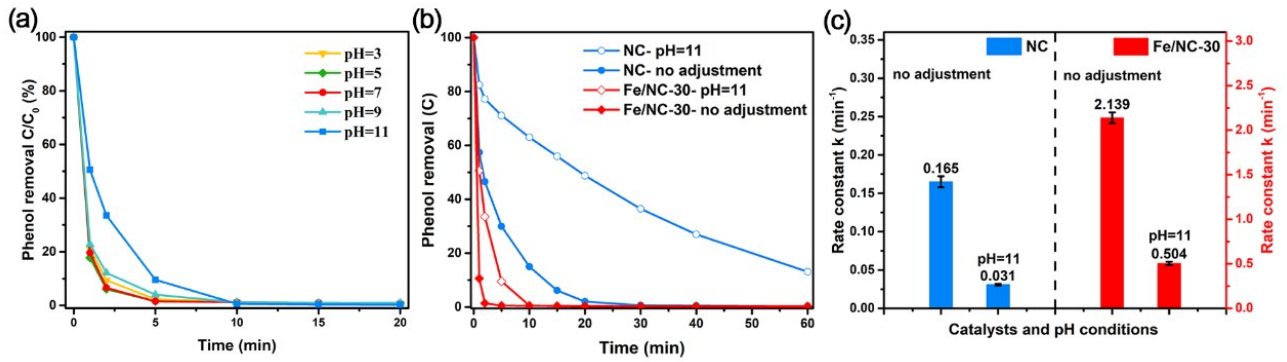

Fig. S12 (a) The effects of initial pH on phenol degradation with Fe/NC-30 as activator. (b) Phenol removal and (c) corresponding reaction rate constants on different pH conditions with Fe/NC-30 and NC as activators. (The reaction conditions: [phenol] = 50 ppm, [activator] = 25 mg/L, [PMS] = 1.0 g/L, T = 25 ºC.)

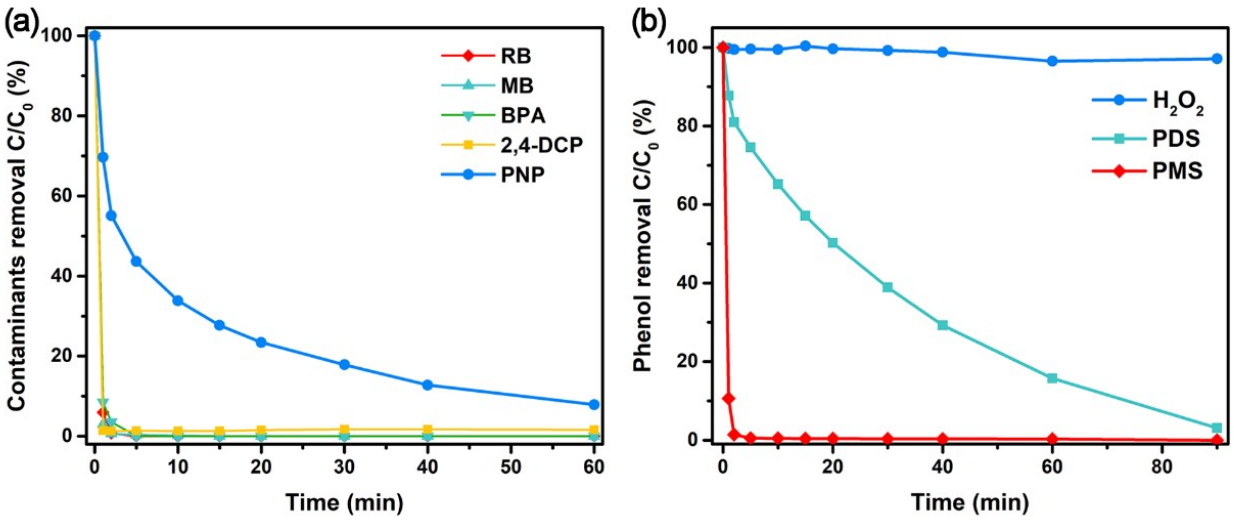

Fig. S13 Degradation performance of (a) different organic contaminants and (b) different oxidants with Fe/NC-30 as activator. (The reaction conditions: [contaminants] = 50 ppm, [activator] = 25 mg/L, [oxidants] = 1.0 g/L, T = 25 ºC.)

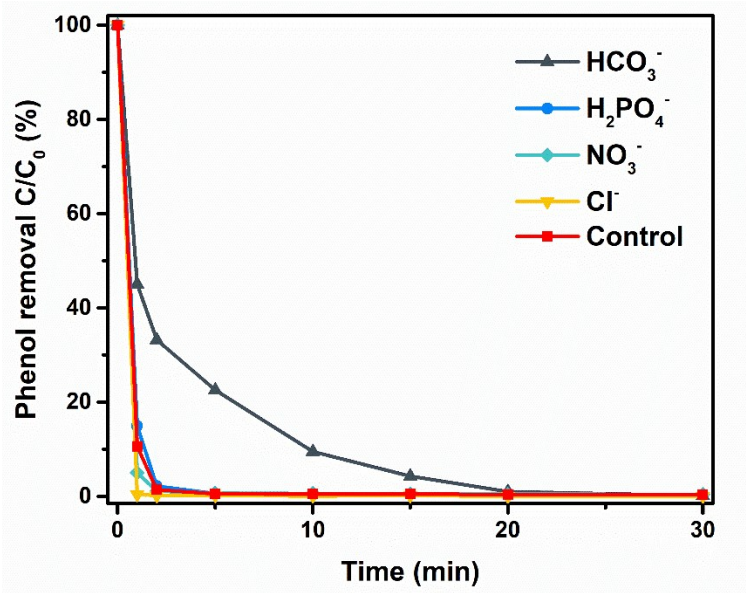

Fig. S14 The effects of different anions on phenol degradation with Fe/NC-30 as activator ([anions] = 10 mM)

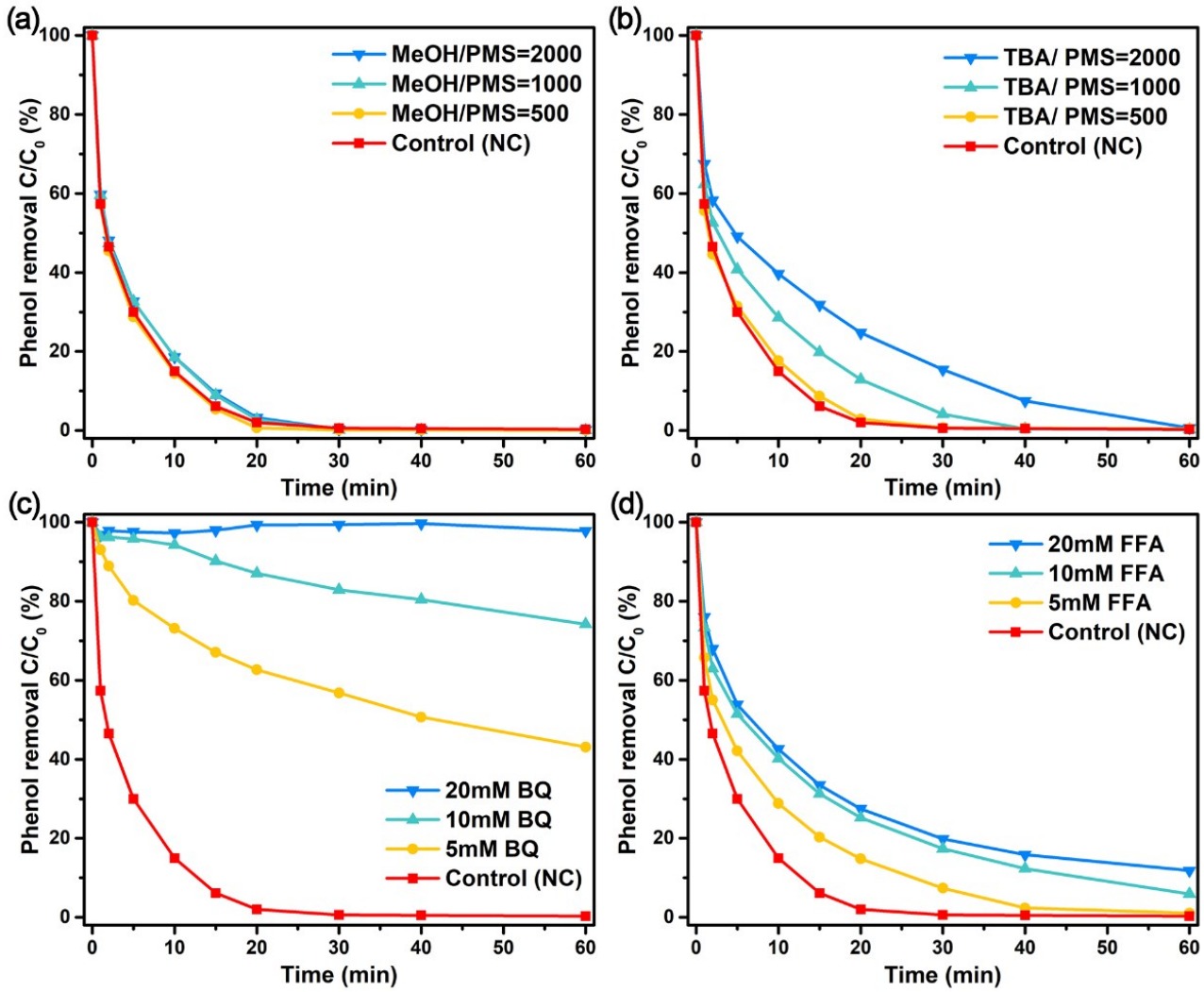

Fig. S15 The effects of (a) MeOH, (b) TBA, (c) BQ and (d) FFA on phenol degradation with NC as activator.

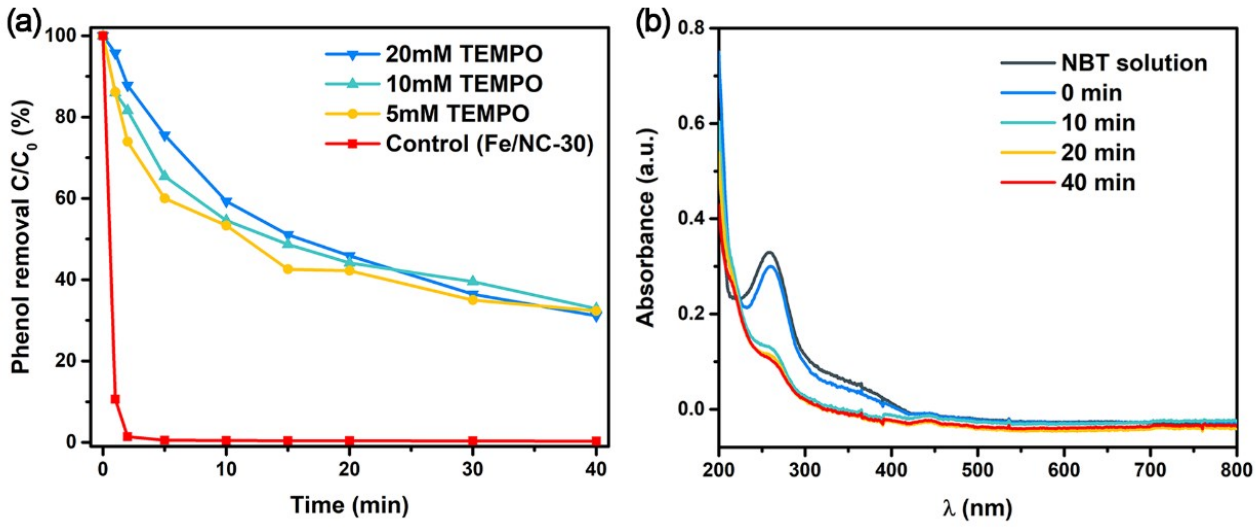

Fig. S16 (a) The effect of TEMPO on phenol degradation with Fe/NC-30 as activator. (b) UV-vis adsorption spectra of NBT

in (Fe/NC-30)/PMS system. (The reaction conditions: [phenol] = 50 ppm, [NBT]=5ppm, [activator] = 25 mg/L, [PMS] = 1.0 g/L, T = 25 ºC.)

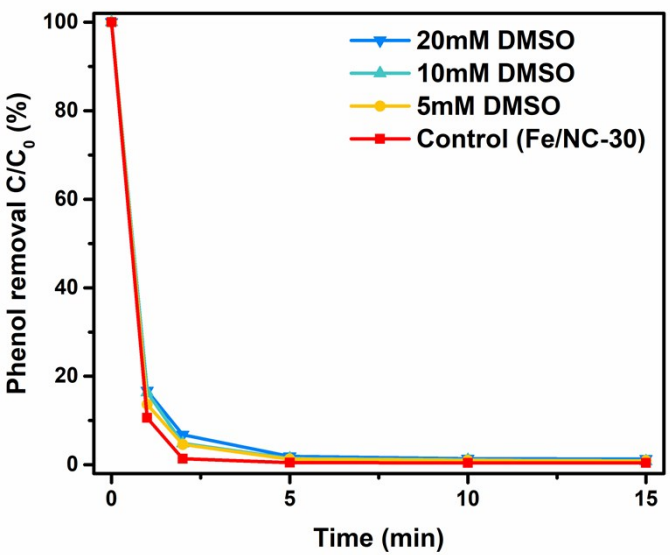

Fig. S17 The effect of DMSO on phenol degradation with Fe/NC-30 as activator.

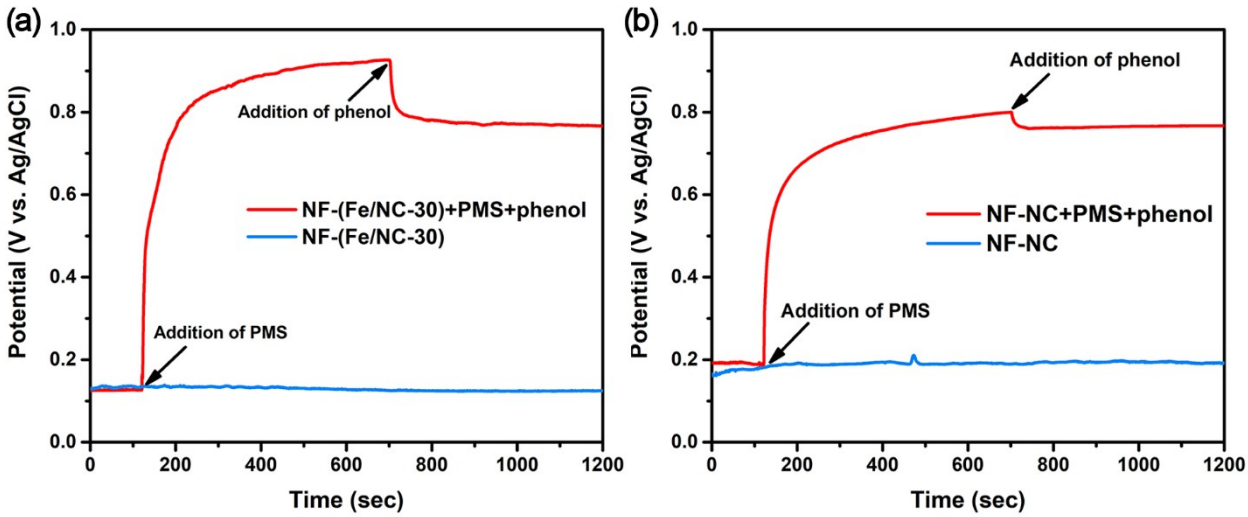

Fig. S18 The chronopotentiometry curves on (a) NF-(Fe/NC-30) and (b) NF-NC electrode under different conditions.

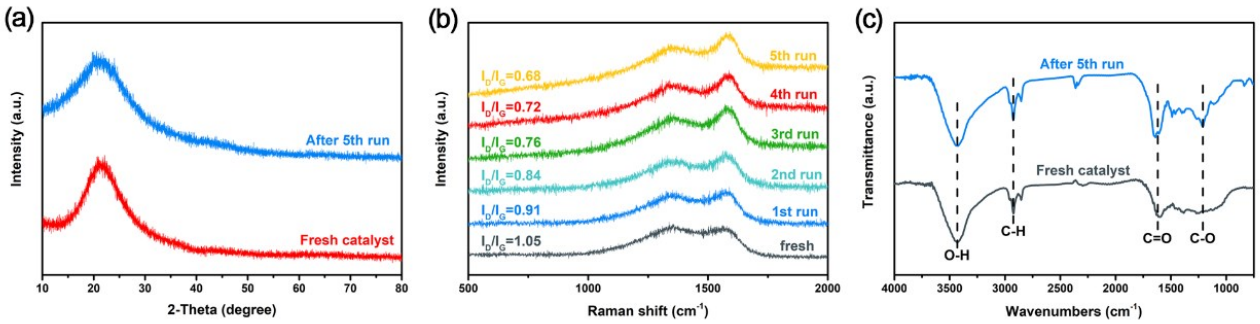

Fig. S19 (a) XRD patterns, (b) Raman spectra and (c) FT-IR spectroscopy of Fe/NC-30 sample before reaction and after

reaction (5th run for XRD and FT-IR, each run for Raman.)

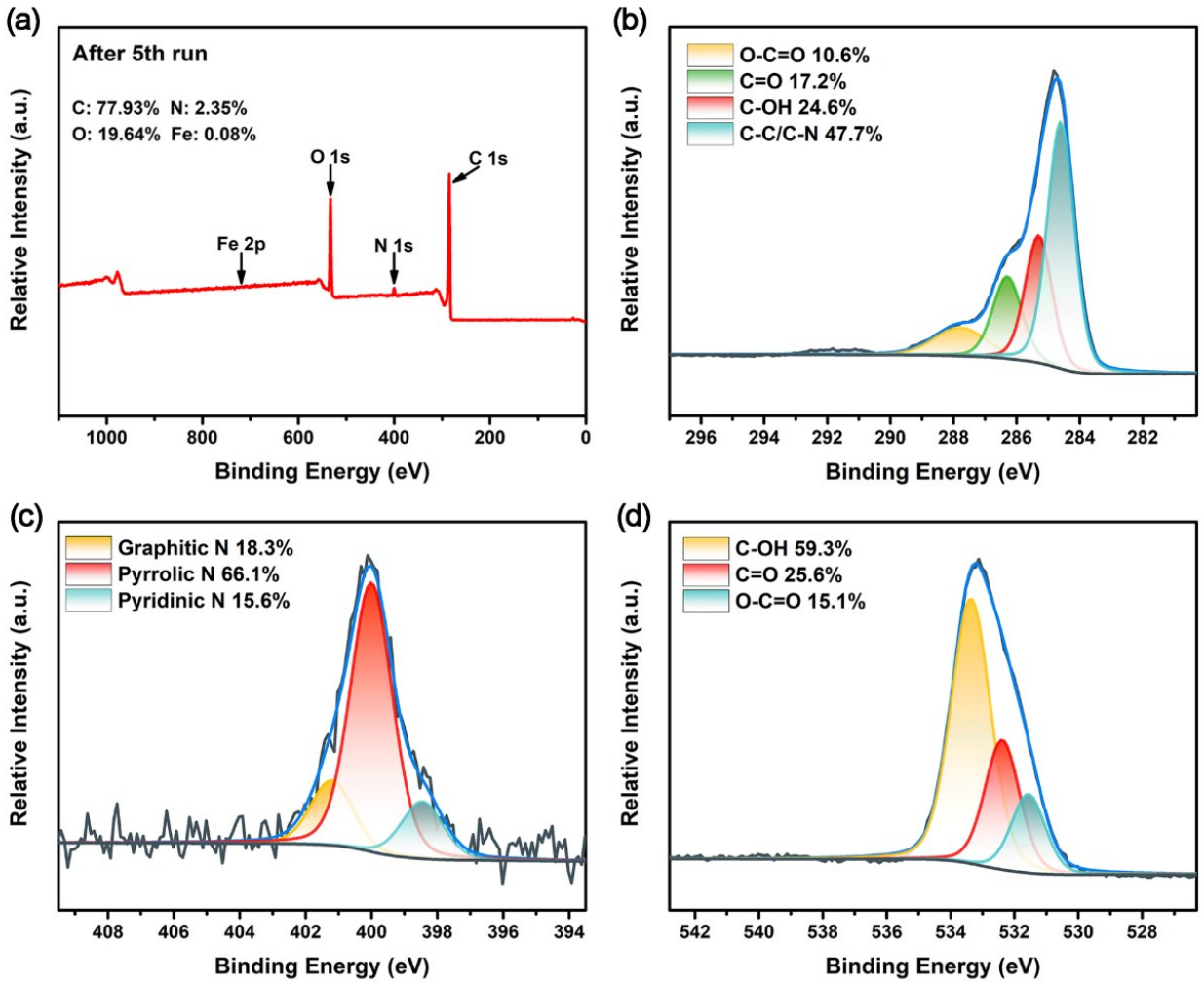

Fig. S20 (a) XPS survey and corresponding (b) C 1s spectra, (c) N 1s spectra and (d) O 1s spectra of Fe/NC-30 after reaction (5th run).

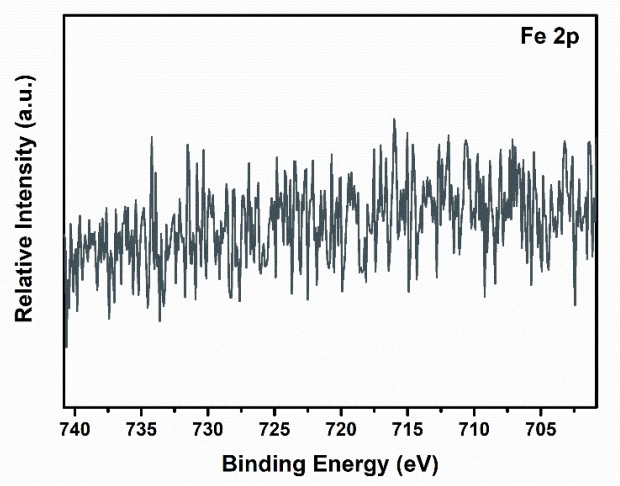

Fig. S21 Fe 2p spectra of Fe/NC-30 after 5th run.

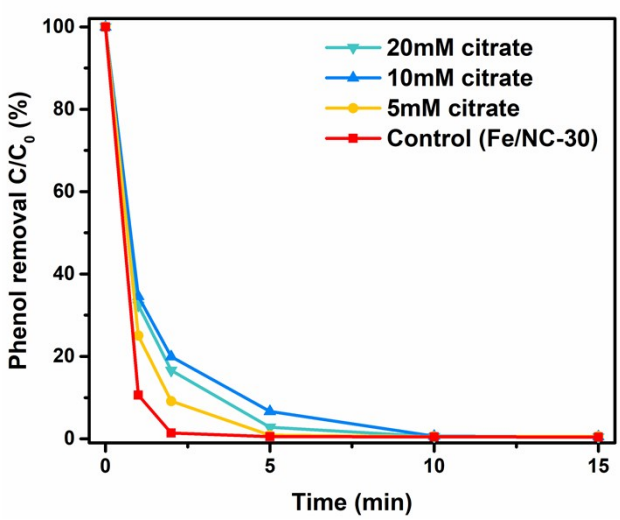

Fig. S22 The effect of citrate on degradation with Fe/NC-30 as activator.

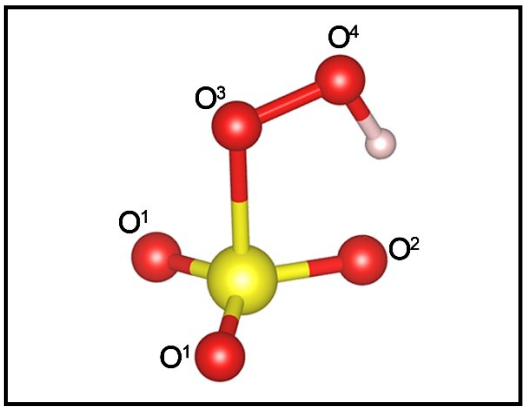

Fig. S23 The model of PMS molecule with labeled O atoms.

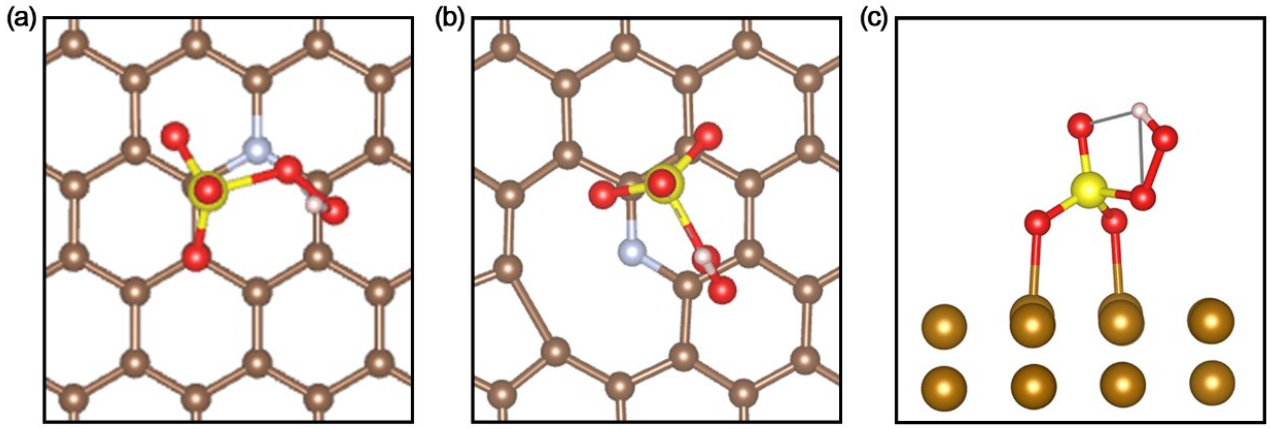

Fig. S24 The fully relaxed adsorption configurations of PMS molecule on (a) graphitic N, (b) pyridinic N and (c) Fe.

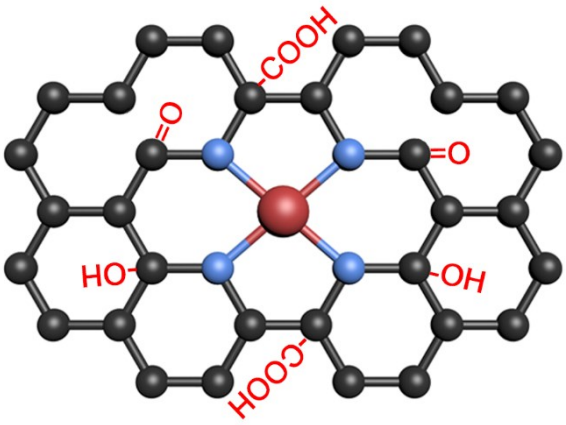

Fig. S25 Oxidation state of Fe-N_4-C_x structure in Fe/NC-30.

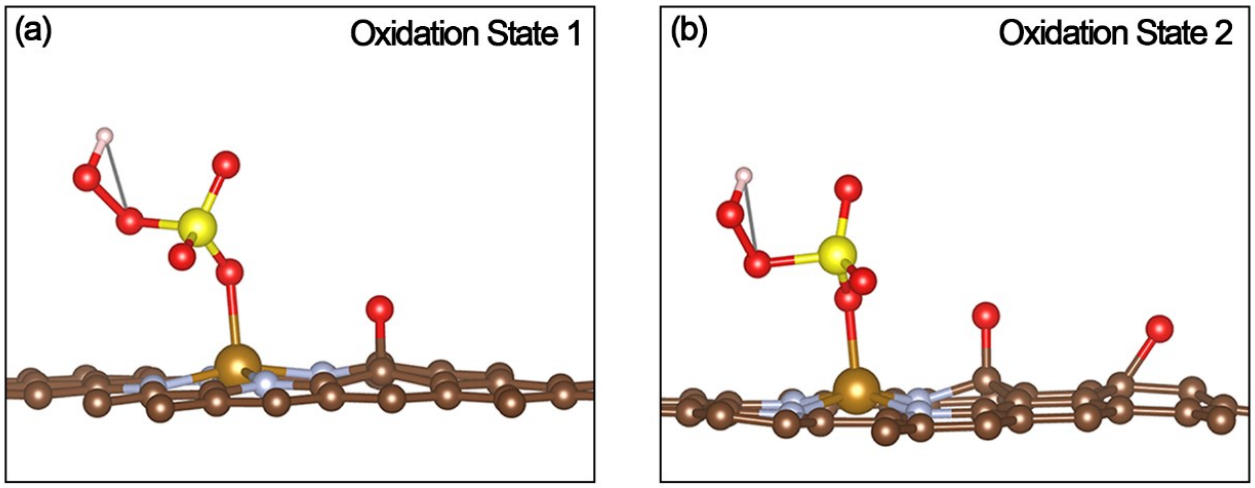

Fig. S26 The PMS adsorption configurations on (a) oxidation state 1 and (b) oxidation state 2 of Fe/N_4-C_x.

Table S1. BET specific surface areas (SSAs) and total pore volume of Fe/NC-30 and NC.

Samples	BET specific surface areas (m^2/g)	
Fe/NC-30	871.4 882.9	877.2 ± 5.7
NC	639.6 640.4	640.0 ± 0.4

Table S2a. Chemical components of Fe/NC-30 and NC obtained by XPS survey.

Samples	C, at%	N, at%	O, at%	Fe, at%
Fe/NC-30	86.45	8.87	4.52	0.16
NC	83.56	9.73	6.72	--

Table S2b. The ratios of different N to total N content in Fe/NC-30 and NC.

Samples	N oxides, at%	Graphitic N, at%	Pyrrolic N, at%	Pyridinic N, at%
Fe/NC-30	9.60	30.47	18.19	41.74
NC	11.62	29.57	21.04	37.76

Table S2c. The ratios of different C to total C content in Fe/NC-30 and NC.

Samples	O-C=O, at%	C=O, at%	C-OH, at%	C-C/C-N, at%
Fe/NC-30	9.81	11.01	28.55	50.63
NC	11.77	9.33	27.99	50.91

Table S2d. The ratios of different O to total O content in Fe/NC-30 and NC.

Samples	C-OH, at%	C=O, at%	O-C=O, at%
Fe/NC-30	21.39	42.66	35.59
NC	22.88	37.41	39.71

Table S3. Best fitting EXAFS data for Fe/NC-30 and reference samples.

Samples	Path	N	R (Å)	σ^2 (Å^2)	ΔE_0 (eV)	R-factor
Fe foil	Fe-Fe_1	8	2.456	0.00585	3.054	0.005
	Fe-Fe_2	6	2.832	0.00494	3.054	
	Fe-Fe_3	12	4.043	0.00947	3.054	
FeO	Fe-O_1	6	2.101	0.01395	2.85	0.003
	Fe-Fe	12	3.074	0.01362	1.17	
	Fe-O_2	8	3.995	0.00841	9.44	
Fe_2O_3	Fe-O	6	1.961	0.01095	7.51	0.008
	Fe-Fe	6	2.983	0.00885	0.96	
Fe/NC-30	Fe-N	3.97±0.38	1.950	0.00519	-6.89	0.004
	Fe-Fe	0.36±0.07	2.524	0.00519	-6.89	

Table S4. The performance comparison of recently reported Fenton-like catalysts for PMS activation and pollutants degradation.

Catalysts (loading, g/L)	Pollutants (mg/L)	PMS g/L	Removal efficiency	Ref.
P-NRGO (0.05)	Phenol (50)	2.0	100% (20 min)	7
PAM-0.5-700 (0.05)	Phenol (20)	2.0	100% (1 min)	8
P-NCC-0.8 (0.05)	Phenol (20)	1.0	100% (10 min)	9
NoCNT-700 (0.1)	Phenol (20)	4.0	100% (20 min)	10
N-PC1000 (0.05)	Naproxen (20)	0.5	100% (30 min)	11
NGA (0.05)	Phenol (20)	2.0	100% (60 min)	12
NC (0.025)	Phenol (50)	1.0	100% (20 min)	This work
p-Mn/ Fe_3O_4 (0.2)	BPA (22.8)	1.23	100% (30 min)	13
Fe-g-C_3N_4 (1.0)	Phenol (9.4)	3.08	100% (15 min)	14
Fe_{SA}-N-C (0.15)	BPA (20)	0.4	100% (20 min)	15
Fe@TpPa-2-700 (0.1)	Orange II (20)	0.40	100% (45 min)	16
FeCo-NC-2 (0.1)	BPA (20)	0.2	100% (4 min)	17
Mn-ISAs@CN (0.2)	BPA (20)	0.2	100% (4 min)	18
MnO_2/$ZnFe_2O_4$ (0.2)	Phenol (20)	2.0	100% (120 min)	19
Co^{2+}@PMAP (0.4)	Phenol (10)	1.8	100% (50 min)	20
Fe_3Co_7@C (0.1)	BPA (20)	0.2	95% (30 min)	21
Fe/Fe_3C@NC (0.2)	4-CP (20)	2.0	100% (210 min)	22
Fe_3O_4-Fe/NC (0.1)	Orange II (50)	0.3	100% (120 min)	23
CoO_x-C (0.1)	Phenol (20)	0.3	100% (60 min)	24
$Fe_1Mn_5Co_4$-N@C (0.1)	BPA (20)	0.2	100% (10 min)	25
$CuFe_2O_4$-Fe_2O_3 (0.2)	BPA (5)	0.36	100% (10 min)	26
Fe_3C@NCNTs/GNS (0.2)	BPA (20)	0.3	100% (60 min)	27
Fe/NC-30 (0.025)	Phenol (50)	1.0	100% (2 min)	This work

Table S5. The stability comparison of recently reported Fenton-like catalysts for PMS activation and pollutants degradation.

Catalysts	Removal efficiency					Ref.
	1st run	2nd run	3rd run	4th run	5th run	
PAM-0.5-700	100% (1 min)	100% (30 min)	83% (90 min)	--	--	8
P-NCC-0.8	100% (10 min)	100% (60 min)	81% (120 min)	51% (120 min)	--	9
Fe_{SA}-N-C	100% (20 min)	98% (30 min)	80% (30 min)	--	--	15
Fe@TpPa-2-700	100% (45 min)	100% (165 min)	100% (255 min)	91.5% (360 min)	--	16
FeCo-NC-2	100% (4 min)	90.5% (6 min)	69.0% (6 min)	--	--	17
Mn-ISAs@CN	100% (4 min)	100% (10 min)	100% (10 min)	96% (10 min)	85% (10 min)	18
Co@NC/CC	100% (6 min)	100% (100 min)	64.4% (160 min)	--	--	28
NC	100% (5 min)	100% (20 min)	100% (40 min)	71.3% (60 min)	--	This work
Fe/NC-30	100% (1 min)	100% (5 min)	100% (10 min)	100% (20 min)	100% (40 min)	This work

Table S6. The mass of activator after each reuse (initial activator dosage is 5 mg, 200 ml phenol solution).

Cycle	Fresh Activator	1st run	2nd run	3rd run	4th run	5th run
Mass (mg)	5.0	8.0	11.6	15.1	18.2	22.6
Variation to last run (mg)	--	3.0	3.6	3.5	3.1	4.4
Variation to fresh activator (mg)	--	3.0	6.6	10.1	13.2	17.6

Table S7. The ratios of different elements to total element content in Fe/NC-30 (fresh activator and activator after 5th run).

Samples	Fresh Activator	After 5th run
Total N, at%	8.87	2.35
N oxides, at%	0.85	0
Graphitic N, at%	2.70	0.43
Pyrrolic N, at%	1.61	1.55
Pyridinic N, at%	3.70	0.37
Total O, at%	4.52	19.64
C-OH, at%	0.97	11.64
C=O, at%	1.93	5.02
O-C=O, at%	1.63	2.97
Total C, at%	86.45	77.93
Total Fe, at%	0.16	0.08

Table S8. The adsorption energy and O-O bond length of several different adsorption configurations of PMS molecule on Fe-N_4 coordination structure.

Adsorption configurations	Adsorption energy (eV)	Q (e)	O-O bond length (Å)
Free PMS	--	--	1.331
Type 1	-1.944	0.799	1.474
Type 2	-1.869	0.819	1.469
Type 3	-1.045	0.716	1.436
Type 4	-1.907	0.764	1.473
Type 5	-1.847	0.792	1.470
Type 6	-1.653	0.742	1.470
Type 7	-1.571	0.851	1.479

Table S9. The adsorption energy and O-O bond length of fully relaxed adsorption configurations of PMS molecule on Fe-N_4, graphitic N, pyridinic N and Fe.

Adsorption configurations	Adsorption energy (eV)	Q (e)	O-O bond length (Å)
Free PMS	--	--	1.331
Fe-N_4	-1.944	0.799	1.474
graphitic N	-2.326	0.952	1.474
pyridinic N	-1.011	0.651	1.427
Fe	-3.098	0.998	1.484

Table S10. The comprehensive average charges of Fe, N and C atoms in Fe-N_4-C_x structure before and after PMS molecule adsorption.

Atom	Before adsorption	After adsorption
Fe atom	+0.878	+1.257
N atoms	-2.530	-2.951
C atoms	+1.821	+2.457

Table S11. The adsorption energy, O-O bond length and electron transfer of PMS adsorption on initial state (Type 1), oxidation state 1 and 2.

Adsorption configurations	Adsorption energy (eV)	Q (e)	O-O bond length (Å)
Free PMS	--	--	1.331
Initial state	-1.944	0.799	1.474
Oxidation state 1	-1.914	0.739	1.469
Oxidation state 2	-1.418	0.743	1.467

References

1 Blochl, *Physical review. B, Condensed matter*, 1994, **50**, 17953-17979.
2 Kresse, Furthmuller, *Physical review. B, Condensed matter*, 1996, **54**, 11169-11186.
3 J.P. Perdew, K. Burke, M. Ernzerhof, *Physical Review Letters*, 1996, **77**, 3865-3868.
4 W. Tang, E. Sanville, G. Henkelman, *J. Phys.-Condes. Matter*, 2009, **21**, 7.
5 K. Momma, F. Izumi, *Journal of Applied Crystallography*, 2011, **44**, 1272-1276.
6 V. Wang, N. Xu, J. Liu, G. Tang, W. Geng, *arXiv:1908.08269*.
7 D. Wu, W.Y. Song, L.L. Chen, X.G. Duan, Q. Xia, X.B. Fan, Y. Li, F.B. Zhang, W.C. Peng, S.B. Wang, *J. Hazard. Mater.*, 2020, **381**, 10.
8 Z. Yang, X.G. Duan, J. Wang, Y. Li, X.B. Fan, F.B. Zhang, G.L. Zhang, W.C. Peng, *ACS Sustain. Chem. Eng.*, 2020, **8**, 4236-4243.
9 J. Wang, Z. Yang, Y. Li, X.B. Fan, F.B. Zhang, G.L. Zhang, W.C. Peng, S.B. Wang, *Carbon*, 2020, **163**, 43-55.
10 X.G. Duan, H.Q. Sun, Y.X. Wang, J. Kang, S.B. Wang, *ACS Catal.*, 2015, **5**, 553-559.
11 J. Wang, X. Duan, J. Gao, Y. Shen, X. Feng, Z. Yu, X. Tan, S. Liu, S. Wang, *Water Res.*, 2020, **185**, 116244.
12 J. Wang, X.G. Duan, Q. Dong, F.P. Meng, X.Y. Tan, S.M. Liu, S.B. Wang, *Carbon*, 2019, **144**, 781-790.
13 J.K. Du, J.G. Bao, Y. Liu, S.H. Kim, D.D. Dionysiou, *Chem. Eng. J.*, 2019, **376**, 9.
14 Y. Feng, C.Z. Liao, L.J. Kong, D.L. Wu, Y.M. Liu, P.H. Lee, K. Shih, *J. Hazard. Mater.*, 2018, **354**, 63-71.
15 Y. Li, T. Yang, S.H. Qiu, W.Q. Lin, J.T. Yan, S.S. Fan, Q. Zhou, *Chem. Eng. J.*, 2020, **389**, 10.
16 Y.J. Yao, H.Y. Yin, M.X. Gao, Y. Hu, H.H. Hu, M.J. Yu, S.B. Wang, *Chem. Eng. Sci.*, 2019, **209**, 13.
17 X.N. Li, X. Huang, S.B. Xi, S. Miao, J. Ding, W.Z. Cai, S. Liu, X.L. Yang, H.B. Yang, J.J. Gao, J.H. Wang, Y.Q. Huang, T. Zhang, B. Liu, *J. Am. Chem. Soc.*, 2018, **140**, 12469-12475.
18 J. Yang, D. Zeng, Q. Zhang, R. Cui, M. Hassan, L. Dong, J. Li, Y. He, *Appl. Catal., B*, 2020, **279**.
19 Y.X. Wang, S. Indrawirawan, X.G. Duan, H.Q. Sun, H.M. Ang, M.O. Tade, S.B. Wang, *Chem. Eng. J.*, 2015, **266**, 12-20.
20 Y.-P. Zhu, T.-Z. Ren, Z.-Y. Yuan, *RSC Adv.*, 2015, **5**, 7628-7636.
21 X.N. Li, A.I. Rykov, B. Zhang, Y.J. Zhangc, J.H. Wang, *Catal. Sci. Technol.*, 2016, **6**, 7486-7494.
22 T. Zeng, M.D. Yu, H.Y. Zhang, Z.Q. He, J.M. Chen, S. Song, *Catal. Sci. Technol.*, 2017, **7**, 396-404.
23 T. Zeng, S.Q. Li, J.A. Hua, Z.Q. He, X.L. Zhang, H.R. Feng, S. Song, *Sci. Total Environ.*, 2018, **645**, 550-559.
24 Y.B. Wang, D. Cao, X. Zhao, *Chem. Eng. J.*, 2017, **328**, 1112-1121.
25 X.N. Li, Z.M. Ao, J.Y. Liu, H.Q. Sun, A.I. Rykov, J.H. Wang, *ACS Nano*, 2016, **10**, 11532-11540.
26 W.D. Oh, Z.L. Dong, Z.T. Hu, T.T. Lim, *J. Mater. Chem. A*, 2015, **3**, 22208-22217.
27 W.J. Ma, N. Wang, Y.C. Du, T.Z. Tong, L.J. Zhang, K.Y.A. Lin, X.J. Han, *Chem. Eng. J.*, 2019, **356**, 1022-1031.
28 Q.Q. Jia, Y. Gao, Y. Li, X.B. Fan, F.B. Zhang, G.L. Zhang, W.C. Peng, S.B. Wang, *Carbon*, 2019, **155**, 287-297.